

Cr₂O₃ thin films grown at room temperature by low pressure laser-CVD

P.M. Sousa¹, A.J. Silvestre^{2a} and O. Conde¹

¹ *Universidade de Lisboa, Faculdade de Ciências, Departamento de Física and ICEMS,
Campo Grande, Ed. C8, 1749-016 Lisboa, Portugal*

² *Instituto Superior de Engenharia de Lisboa and ICEMS, R. Conselheiro Emídio Navarro 1,
1959-007 Lisboa, Portugal*

Abstract

Chromia (Cr₂O₃) has been extensively explored aiming the development of widespread industrial applications, due to the convergence of a variety of mechanical, physical and chemical properties in one single oxide material. Various methods have been used for large area synthesis of Cr₂O₃ films. However, for selective area growth and growth on thermally sensitive materials, laser-assisted chemical vapour deposition (LCVD) can be applied advantageously.

Here we report on the growth of single layers of pure Cr₂O₃ onto sapphire substrates at room temperature by low pressure photolytic LCVD, using UV laser radiation and Cr(CO)₆ as chromium precursor. The feasibility of the LCVD technique to access selective area deposition of chromia thin films is shown. Best results were obtained for a laser fluence of 120 mJ cm⁻² and a partial pressure ratio of O₂ to Cr(CO)₆ of 1.0. Samples grown with these experimental parameters are polycrystalline and their microstructure is characterised by a high density of particles whose size follows a lognormal distribution. Deposition rates of 0.1 nm s⁻¹ and mean particle sizes of 1.85 µm were measured for these films.

Keywords: Cr₂O₃ thin films, low pressure LCVD, microstructure, particle size distribution

PACS: 81.05.Je; 81.15.-z; 81.16.Mk; 82.50.Hp

^a Corresponding author: e-mail: asilvestre@deq.isel.ipl.pt

1. Introduction

Among the different chromium oxide solid phases, Cr_2O_3 is the most stable existing in a wide domain of temperature and pressure [1]. It exhibits many attractive tribological properties, such as high hardness (29.5 GPa) and high melting point ($\sim 2300^\circ\text{C}$) combined with chemical inertness, low friction coefficient, high wear resistance, and high temperature oxidation resistance [2,3]. Regarding magnetic behaviour, Cr_2O_3 is antiferromagnetic with a Néel temperature of 307 K [4]; however, the antiferromagnetic character can be changed to weak ferromagnetism [5] and even superparamagnetism [6] when chromia nanoparticles are considered. On the other hand, despite its intrinsic insulator nature, Cr_2O_3 films can present either *p*-type or *n*-type semiconductor behaviour, depending on the growth conditions [7]. It also shows a high solar absorption coefficient and low thermal emissivity [8]. The confluence of all these properties in one unique material makes Cr_2O_3 a key material regarding the development of a broad range of industrial applications.

A wide variety of chemical and physical methods have been used for large area synthesis of Cr_2O_3 films, e.g. CVD at either atmospheric [9,10] or low pressure [11], plasma enhanced CVD (PECVD) [12,13], electrodeposition [14], metal oxidation [15], chemical spray pyrolysis [16], RF magnetron sputtering [17,18], molecular beam epitaxy [19,20] and atomic layer deposition [21].

Laser-assisted chemical vapour deposition (LCVD) can be an advantageous technique whenever selective area growth or thermally sensitive substrate materials are required. Dowben and co-authors [22] achieved the synthesis of films containing both Cr_2O_3 and CrO_2 on Si(111) wafers, in a low pressure of $\sim 10^{-5}$ mbar static reactive atmosphere, by using a nitrogen laser ($\lambda = 337$ nm) and $\text{Cr}(\text{CO})_6$ as chromium precursor. Looking for a better efficiency of the deposition process, we have previously explored dynamic atmospheres at higher pressure ($\sim 10^{-1}$ mbar) using KrF laser radiation ($\lambda = 248$ nm) for which the $\text{Cr}(\text{CO})_6$ absorption cross section is much higher than for the nitrogen laser. In such experimental conditions biphasic films consisting of Cr_2O_3 and CrO_2 were also deposited [23].

Here we present results on the synthesis of pure Cr_2O_3 films grown onto c-cut sapphire at room temperature by LCVD at low pressure, using KrF laser radiation to promote the photodissociation of $\text{Cr}(\text{CO})_6$ in dynamic atmospheres containing oxygen.

2. Experimental details

The experimental apparatus used for the depositions consists of a KrF excimer laser (248 nm wavelength, 30 ns pulse duration), a stainless steel high vacuum reaction chamber, a high vacuum pumping system and a gas system for delivering the reactants to the reaction chamber. The KrF laser working at a repetition rate of 10 Hz irradiated the Al₂O₃ (0001) substrates at perpendicular incidence. The beam spot size on the substrate's surface was 8.2 mm². Prior to any deposition experiment the reactor was evacuated to a base pressure lower than 2×10^{-6} mbar. All the deposition experiments were conducted at room temperature (RT) in dynamic gas regime, at a constant total pressure of 4.5×10^{-5} mbar and for a total deposition time of 4 hours. Cr(CO)₆ powder, whose vapour pressure as a function of temperature is given by $\log_{10} p_{\text{Cr(CO)}_6} = 12.75 - 3285/T$ [24], where $p_{\text{Cr(CO)}_6}$ is in Pa and T in K, was sublimated at 22 °C in a controlled temperature stainless steel cell connected to the LCVD reaction chamber. Its flow rate was adjusted by the pressure difference between the reactor and the cell. The O₂ flow rate was varied in the range 0.02 - 0.2 sccm, using a highly sensitive mass flow controller.

The laser fluence, F , and the partial pressure ratio of O₂ to Cr(CO)₆, $R = p_{\text{O}_2}/p_{\text{Cr(CO)}_6}$, were correlated with the phase composition, degree of crystallinity, deposition rate, and microstructure of the as-deposited films. The structural analysis was carried out by X-ray diffraction with Cu K α radiation and by micro-Raman spectroscopy using the 514.5 nm excitation line of an Ar⁺ laser. The full-width at half-maximum (FWHM) of the diffraction lines were calculated by fitting with a pseudo-Voigt function while the Raman shifts were obtained by fitting the Raman bands with a Lorentzian function. The morphology and microstructure of the films were analysed by scanning electron microscopy (SEM), and their thickness measured with a Dektak stylus profilometer. Particle size distributions were calculated by digital analysis of the SEM micrographs recorded from the surface of the films.

3. Results and discussion

Because the substrate material is transparent to the KrF laser radiation and a low Cr(CO)₆ partial pressure was used, the deposition can be classified as a nearly pure photolytic surface mediated process. Only at the substrate level some scattering of the laser radiation was observed. As it will be shown, the deposition of Cr₂O₃ was achieved within a very narrow range of the experimental parameters, although reproducibility was excellent. Best results were obtained for $F = 120 \text{ mJ cm}^{-2}$ and $R = 1.0$. Films deposited using these experimental

conditions are greenish, well adherent to the substrate and well crystallized, their thickness following the laser beam transversal Gaussian profile, as can be seen in figure 1. Films deposited at $60 \leq F < 120 \text{ mJ cm}^{-2}$ present rather low deposition rates and do not completely cover the irradiated region of the substrate; for $F < 60 \text{ mJ cm}^{-2}$ and/or $R > 2.9$ no deposition was observed. On the other hand, when using laser fluences higher than 125 mJ cm^{-2} substrate damage and/or film ablation occur, no matter the R values employed.

The micro-Raman spectra and the XRD patterns of the films deposited at $F = 120 \text{ mJ cm}^{-2}$ as a function of the oxygen to chromium hexacarbonyl partial pressure ratio are depicted in figure 2. A set of bands matching the Raman active modes of Cr_2O_3 [25-27] can be seen in figure 2a. The diffractograms of the same films (fig. 2b) show that those deposited at $R = 0.3$ and 1.0 are polycrystalline, presenting several well resolved diffraction lines that could only be indexed to the rhombohedral $\alpha\text{-Cr}_2\text{O}_3$ phase (JCPDS file n° 38-1479). No traces of other chromium oxide secondary phases were observed. Mean crystallite sizes of 146 nm and 95 nm were estimated for the films grown at $R = 0.3$ and 1.0 , respectively, using the (104) reflection at $2\theta = 33.602^\circ$ and Scherrer's equation [28]. In contrast, the intensity of the diffraction lines of the films grown at $R = 0.1$ and 2.9 are very low, suggesting a lower amount of deposited material i.e., lower deposition rate and/or the growth of a prominent amorphous phase. However, the analysis of the micro-Raman spectra of the films (fig. 2a) shows that the A_{1g} band is similar for the three films grown with $R \geq 0.3$ and only for the film deposited at $R = 0.1$ is this band broader and red shifted, which is usually associated to structural disorder [26]. Therefore, the preponderant factor determining the observed low intensity of the diffraction patterns for the films grown at $R = 0.1$ and 2.9 should be the lower growth rate. Figure 3 shows the dependence of film thickness on the R parameter of the films grown at $F = 120 \text{ mJ cm}^{-2}$. The thickness increases with R up to an estimated $R \sim 1.5$, decreasing sharply for higher pressure ratios. Films grown at R values of 0.1 and 2.9 have similar thicknesses. Films deposited with $R = 1.0$ are those with the highest measured deposition rate, reaching values of 0.1 nm s^{-1} , one order of magnitude higher than the deposition rates reported for Cr_2O_3 films deposited by PECVD at 300°C , using the same Cr precursor [13].

The influence of R on the deposition trend may be understood taking into account the interactions between the reactive species on the surface of the substrate. Parnis *et al.* [29] reported that the reaction rate of Cr with O_2 , where Cr results from the photodissociation of $\text{Cr}(\text{CO})_6$, increases linearly as a function of p_{O_2} . Thus, a linear increase of the chromium oxide deposition rate with increasing R would be expected if the interactions of the substrate surface

with the gaseous atmosphere were irrelevant. In fact, the deposition is initiated by one-photon dissociation of the hexacarbonyl to Cr(CO)_x photoproducts which are adsorbed on the substrate surface within the laser beam spot and further dissociate to Cr [30]. When O_2 is present, the final reaction step is the surface reaction to form the chromium oxides. Although in the molecular state, O_2 is also competing for the same adsorption sites as Cr(CO)_x . The decrease in the available surface adsorption sites for the Cr precursor with increasing oxygen pressure leads to the decrease of the chromium oxide deposition rate. Therefore, the balance between these two opposite effects explain the non-linear behaviour of the Cr_2O_3 deposition rate, in particular the existence of a maximum measured for $R=1.0$. On the other hand, low oxygen partial pressure regimes favour the growth of oxygen deficient films with higher structural disorder. This explains the broadening and red shift of the A_{1g} Raman peak observed for the sample deposited at $R=0.1$, in comparison with the film grown at $R=2.9$, despite their similar thicknesses.

The effect of decreasing laser fluence on the growth of Cr_2O_3 films was studied by conducting new deposition experiments with different R 's using laser fluences of 80 mJ cm^{-2} and 60 mJ cm^{-2} . The very low intensity of the diffraction lines in the XRD patterns (not shown), and the indexing of Al_2O_3 peaks (substrate material) in the micro-Raman spectra (fig. 4) of the films deposited with these fluences are a clear indication that the deposition rate decreases significantly with decreasing laser fluence. Actually, it was not possible to determine reliable thickness values for these films since often they do not fully cover the irradiated zone of the substrate. In particular for $F=60 \text{ mJ cm}^{-2}$ and $R=2.9$ no deposition was observed. Regarding phase composition, the micro-Raman spectra presented in figure 4 show that the laser fluence has no significant effect on the material synthesised as no other phases besides Cr_2O_3 were identified.

Figure 5 depicts the FWHM of the Cr_2O_3 A_{1g} Raman shift as a function of R for three different laser fluences. The films deposited at $F=120 \text{ mJ cm}^{-2}$ and $R=1.0$ show the narrowest A_{1g} peaks and thus are the ones with the highest degree of crystallinity. Given the results described above, we turned our attention to the microstructure of the films deposited at laser fluence of 120 mJ cm^{-2} . Particle size and particle size distribution are important microstructural attributes of thin films since they can strongly affect the mechanical and tribological, the chemical, optical and physical properties. The microstructure of the as-grown Cr_2O_3 films was studied by SEM in bright field mode. The films consist of a high density of irregular shaped particles, as can be seen from the micrographs depicted in figure 6 for

different R values. In order to evaluate the mean particle size and to build the size distribution histograms of the as-deposited films, the length of about 400 particles was measured. The particle size distributions were obtained using the cumulative percentage method [31]. The histograms as well as their cumulative percentage for each R value are also presented in figure 6. The particle size of the samples grown at $R=2.9$ and 1.0 follow a lognormal distribution with a mean particle size of $1.76\text{ }\mu\text{m}$ ($\sigma=0.29\text{ }\mu\text{m}$) and $1.85\text{ }\mu\text{m}$ ($\sigma=0.24\text{ }\mu\text{m}$), respectively, where σ refers to the standard deviation. The latter result shows that for the film grown at $R=1.0$, the particles are composed of about twenty nanocrystallites, according to the size of the coherent diffracting domains calculated from the XRD pattern of this sample. Furthermore, the lognormal distribution obtained for these two films strongly support that they grow basically via a particle diffusion mechanism and subsequent coalescence [32]. Different particle distribution histograms were found for the samples deposited at lower oxygen partial pressure. Films deposited with $R=0.3$ show a rather flat particle size distribution and thus a high microstructure heterogeneity. A mean particle size of $2.02\text{ }\mu\text{m}$ ($\sigma=0.74\text{ }\mu\text{m}$) was estimated for this sample. On the other hand, films deposited with $R=0.1$ show a bimodal particle size distribution which can be endorsed to the coexistence of crystallized particles with amorphous regions and/or with aggregates not fully crystallized, in agreement with the higher structural disorder observed for the films grown at low oxygen partial pressure, as previously described. In this case an average particle size of $1.70\text{ }\mu\text{m}$ ($\sigma=0.36\text{ }\mu\text{m}$) for the smaller particles and $2.72\text{ }\mu\text{m}$ ($\sigma=0.12\text{ }\mu\text{m}$) for the larger ones were obtained. Altogether, these results show that particle size and particle size distribution are strongly dependent on the reactant atmosphere composition used to grow the Cr_2O_3 single phase layers. For the majority of thin film applications it is crucial to have a particle size as homogeneous as possible and thus a narrow particle size distribution. This is indeed the case of the samples grown with R values of 2.9 and 1.0 , in particular the former one for which a lower particle size standard deviation was determined.

3.3 Conclusions

We have studied the synthesis of Cr_2O_3 thin films produced at room temperature by low pressure LCVD, using KrF laser radiation to promote the photodissociation of $\text{Cr}(\text{CO})_6$ in dynamic atmospheres containing O_2 . Although the deposition was reached within a very narrow range of the experimental parameters, the ability of this technique to achieve selective area growth of highly pure polycrystalline chromia was established. It was shown that the

deposition rate and the degree of crystallinity of the as-deposited material increase with increasing laser fluence. On the other hand, it was shown that oxygen is essential for the growth of fully crystalline Cr_2O_3 , despite appearing to compete with the $\text{Cr}(\text{CO})_6$ photoproducts for the surface adsorption sites and thus the need for a fine balance between the partial pressures of both reactants. It was also shown that the film particle size distribution strongly depends on the O_2 to $\text{Cr}(\text{CO})_6$ pressure ratio, low oxygen partial pressures inducing larger particle size and wider particle size distribution. Best results were obtained for $F=120 \text{ mJ cm}^{-2}$ and $R=1.0$. Films deposited using these experimental parameters are polycrystalline with a narrow lognormal particle size distribution which reflects their microstructural homogeneity. A deposition rate of 0.1 nm s^{-1} and mean particles size of $1.85 \text{ }\mu\text{m}$ with standard deviation of $0.24 \text{ }\mu\text{m}$ were measured in such films.

Acknowledgements

The authors gratefully acknowledge the financial support of Fundação para a Ciência e Tecnologia (FCT) under contract POCTI/CTM/41413/2001. P.M. Sousa also acknowledges FCT for a PhD grant (BD16567/2004).

References

1. B. Kubota, J. Am. Ceram. Soc. 44 (1960) 239
2. J.L. Zang, J. Huang and C. Ding, J. Therm. Spray Technol. 7 (1998) 242.
3. E. Celik, C. Tekmen, I. Ozdemir, H. Cetinel, Y. Karakas, S.C. Okumus, Surf. Coat. Technol. 174/175 (2003) 1074.
4. T. Yu, Z.X. Shen, J. He, W. X. Sun, S. H. Tang, J.Y. Lin, J. Appl. Phys. 93 (2003) 3951.
5. S.A. Makhlof, J. Magn. Magn. Mater., 272/276 (2004) 1530.
6. U. Balachandran, R.W. Siegel, Y.X. Liao, T.R. Askew, NanoStructured Materials 5 (1995) 505.
7. P. Kofstad, K.P. Lillerud, J. Electrochem. Soc. 127 (1980) 2410.
8. T. Maruyama, H. Akagi, J. Electrochem. Soc. 143 (1996) 1955.
9. R.S. Boorse, J.M. Burlitch, Chem. Mater. 6 (1994) 1509.

10. T. Maruyama, H. Akagi, J. Electrochem. Soc. 143 (1996) 1955.
11. F. Barradas-Olmos, J.R. Vargas-Garcia, J.J. Cruz-Rivera, Mater. Sci. Forum 386 (2002) 353.
12. F.K. Perkins, C. Hwang, M. Onellion, Y.G. Kim, P.A. Dowben, Thin Solid Films 198 (1991) 317.
13. J. Wang, A. Gupta, T.M. Klein, Thin Solid Films 516 (2008) 7366.
14. G. Gheorghies, L. Gheorghies, J. Optoelectronics and Advanced Materials 3 (2001) 107.
15. Y. Ito, K. Kushida, H. Takeuchi, J. Cryst. Growth 112 (1991) 427.
16. S. Noguchi, M. Mizuhashi, Thin Solid Films 77 (1981) 99.
17. X. Pang, K. Gao, F. Luo, H. Yang, L. Qiao, Y. Wang, A.A. Volinsky, Thin Solid Films 516 (2008) 4685.
18. S. Sasaki, Y.F. Zhang, O. Yanagisawa, and M. Izumi, J. Magn. Mater. **310** (2007) 1008.
19. P. Borisov, A. Hochstral, V.V. Shvartsman, W. Kleemann, P.M. Hauck, Integrated Ferroelectrics 99 (2008) 69.
20. M.A. Henderson, S.A. Chambers, Surf. Sci. 449 (2000) 135.
21. H. Mändar, T. Uustare, J. Aarik, A. Tarre, A. Rosental, Thin Solid Films 515 (2007) 4570.
22. R. Cheng, C.N. Borca, P.A. Dowben, S. Stadler, Y.U. Idzerda, Appl. Phys. Letters 78 (2001) 521.
23. P.M. Sousa, A.J. Silvestre, N. Popovici, O. Conde, Appl. Surf. Sci. 247 (2005) 423.
24. M. M. Windsor, A.A. Blanchard, J. Am. Chem. Soc. 56 (1934) 823.
25. J. Mougín, T.L. Bihan and G. Lucazeau, J. Phys. Chem. Solids 62 (2001) 553.
26. J. Zuo, C. Xu, B. Hou, C. Wang, Y. Xie, Y. Qian, J. Raman Spectroscopy 27 (1996) 921.
27. S.I. Dolgaev, N.A. Kirichenko, G.A. Shafeev, Appl. Surf. Sci. 138/139 (1999) 449.
28. B.D. Cullity, S.R. Stock, Elements of X-ray diffraction, 3rd edition, Prentice-Hall, Inc., New Jersey, 2001, p. 170.
29. J.M. Parnis, S.A. Mitchell, P.A. Hackett, J. Phys. Chem. 94 (1990) 8152.

30. G.W. Tyndall, R.L. Jackson, J. Am. Chem. Soc. 109 (1987) 582.
31. M. Vopsaroiu, G.V. Fernandez, M.J. Thwaites, J. Anguita, P.J. Grundy, K.O.'Grady, J. Phys. D: Appl. Phys. 38 (2005) 490.
32. J. Soderlund, L.B. Kiss, G. A. Niklasson, C.G. Granqvist, Phys. Rev. Letters. 80 (1998) 2386.

Figure captions

Figure 1 - Thickness profile of a film deposited with $F=120 \text{ mJ cm}^{-2}$ and $R=1.0$.

Figure 2 - a) Micro-Raman spectra and b) θ - 2θ XRD patterns of films deposited with $F=120 \text{ mJ cm}^{-2}$ and different R values.

Figure 3 - Film thickness as a function of R for $F=120 \text{ mJ cm}^{-2}$; (---) fitting curve with a 2nd order polynomial.

Figure 4 - Micro-Raman spectra of films deposited using a) $F=80 \text{ mJ cm}^{-2}$ and b) $F=60 \text{ mJ cm}^{-2}$, at different R values (bold face figures). S refers to the substrate.

Figure 5 - Full-width at half-maximum of the Cr_2O_3 A_{1g} Raman band vs. R values for films deposited at different laser fluences.

Figure 6 - SEM micrographs of the surface of films deposited with $F=120 \text{ mJ cm}^{-2}$ and a) $R=2.9$; b) $R=1.0$; c) $R=0.3$; d) $R=0.1$. The corresponding particle size distribution histograms are displayed in the right side of each SEM image. A lognormal distribution function was used to fit the data of films a) and b).

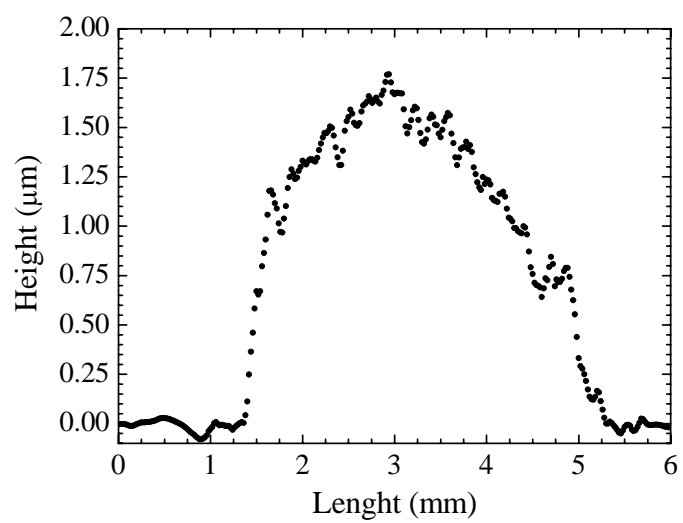


Figure 1

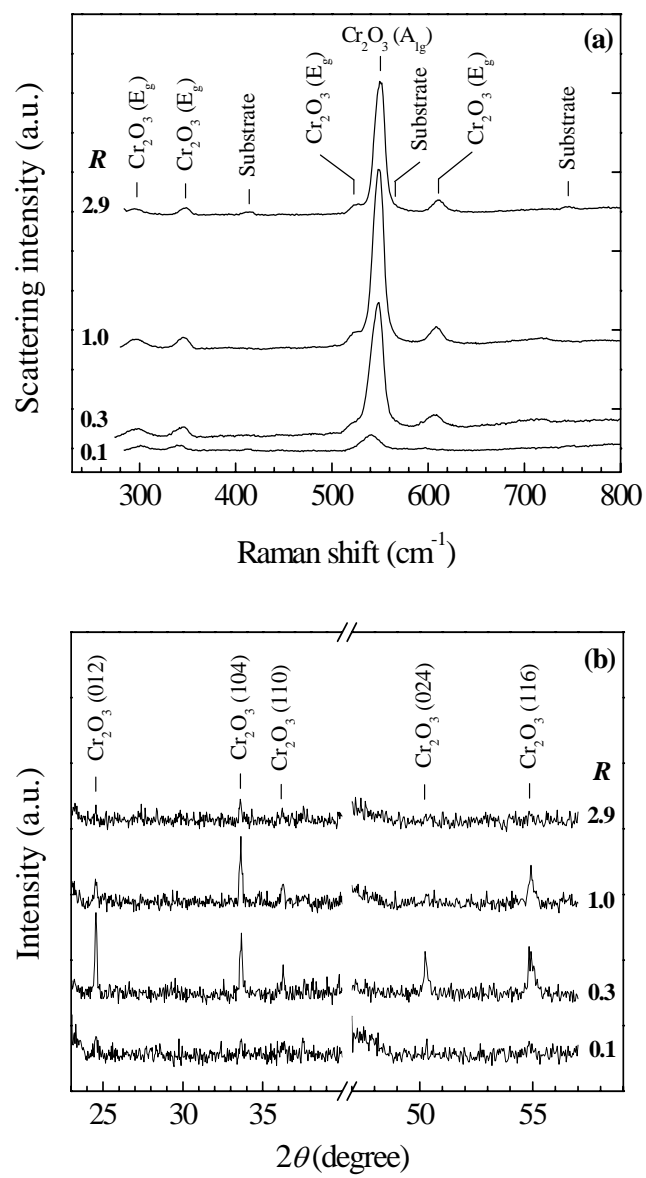


Figure 2

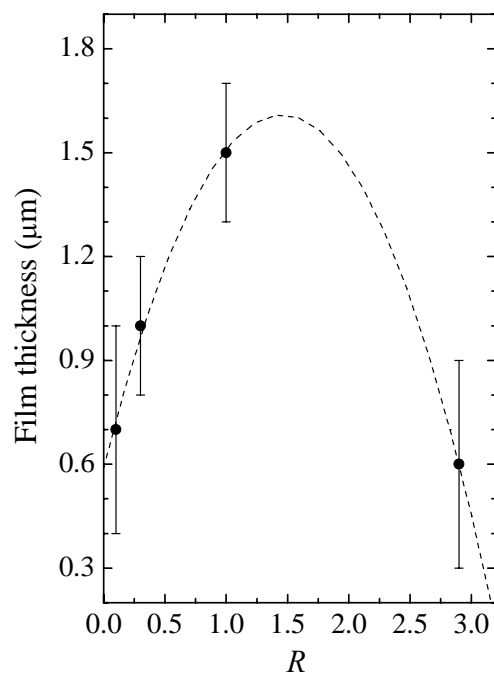


Figure 3

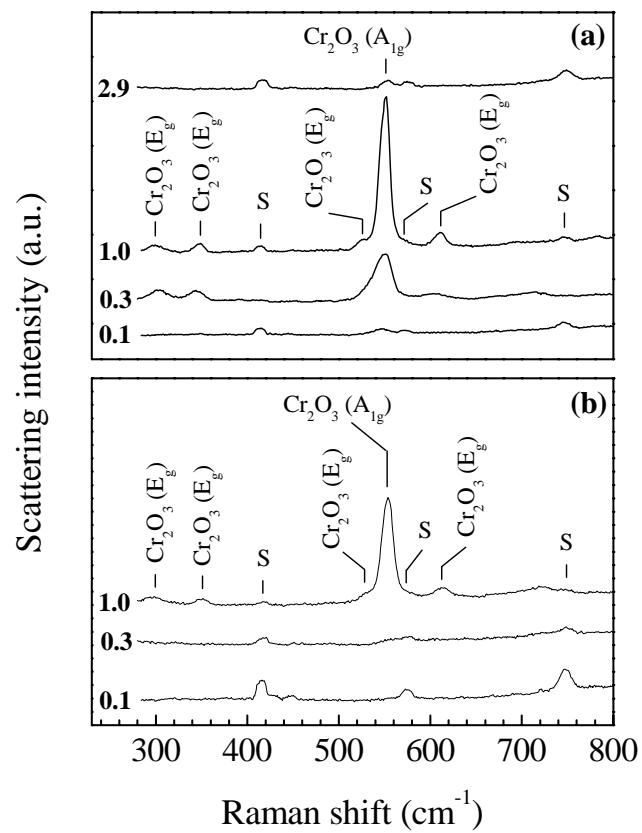


Figure 4

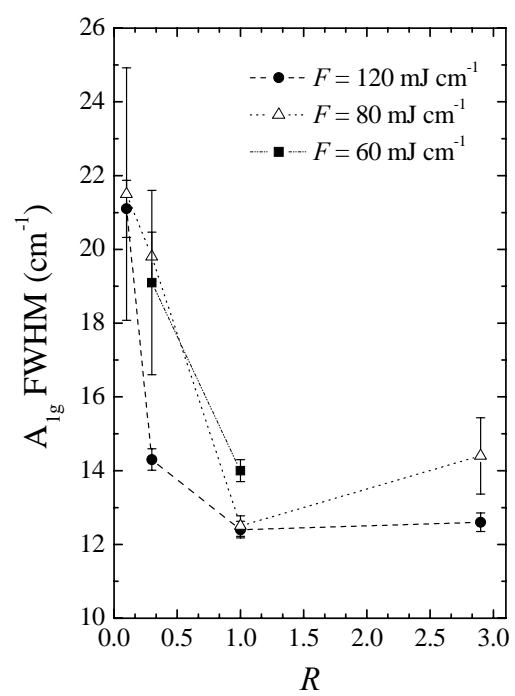


Figure 5

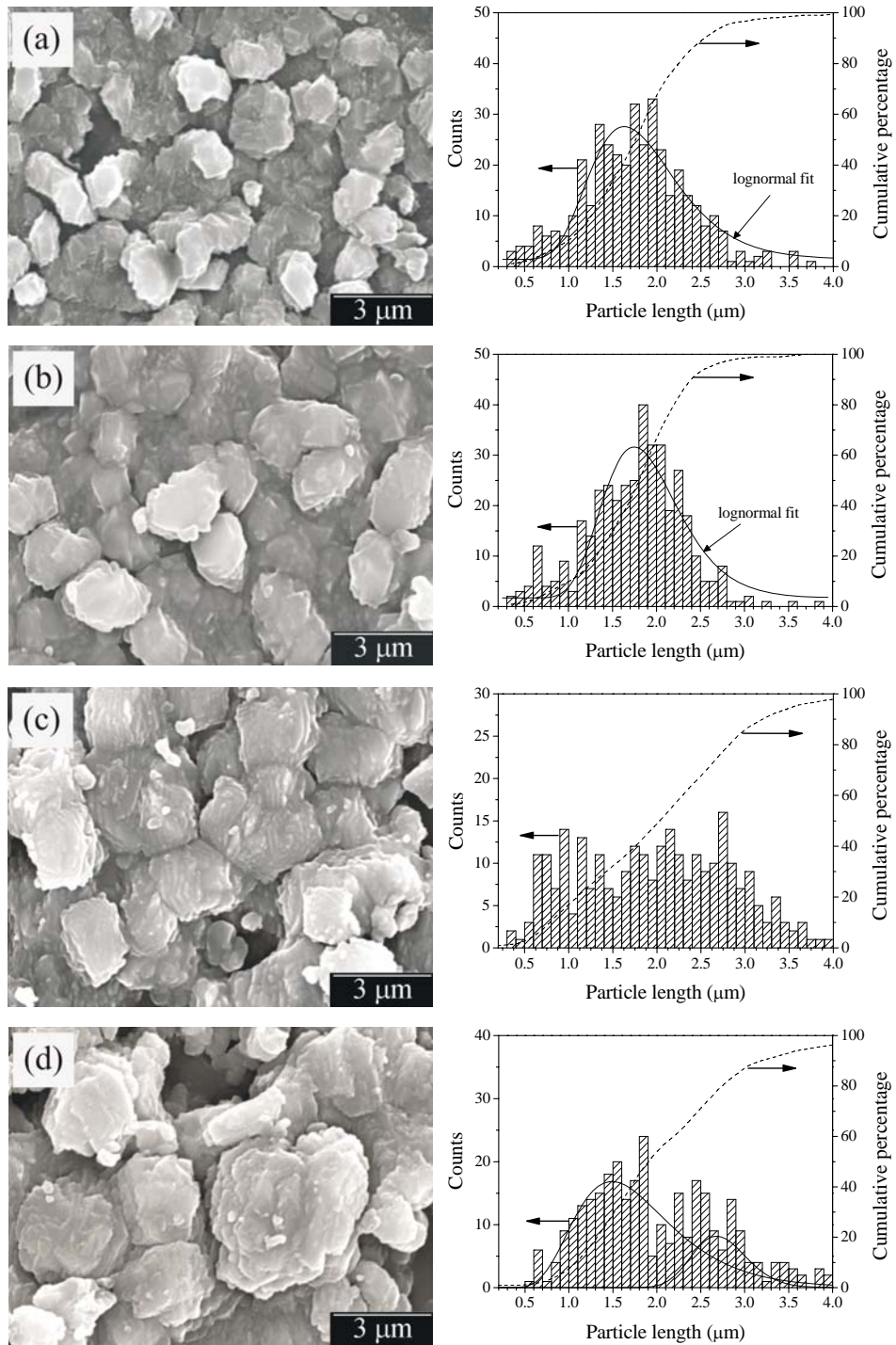


Figure 6